Research Paper

Design and Analysis of Ultrasonic Composite Transducer with a Quarter-wave Taper Transition Horn

Tao CHEN[(1), (2)], Hongbo LI[(1), (2)]*, Qihan WANG[(1), (2)], Junpeng YE[(1), (2)]

[(1)] *School of Mechanical and Electronic Engineering*
Wuhan University of Technology
Wuhan 430070, P.R.China

[(2)] *Hubei Digital Manufacturing Key Laboratory*
Wuhan University of Technology
Wuhan 430070, P.R.China
*Corresponding Author e-mail: lihb01371@163.com

Based on the electromechanical equivalent circuit theory, equations related to the resonance frequency and the magnifying coefficient of a quarter-wave vibrator and a quarter-wave taper transition horn were deduced, respectively. A series of 3D models of ultrasonic composite transducers with various conical section length was also established. To reveal the influences of the conical section length and the prestressed bolt on the dynamic characteristics (resonance frequency, amplitude, displacement node, and the maximum equivalent stress) of the models and the design accuracy, finite element (FE) analyses were carried out. The results show that the addition of prestressed bolt increases the resonance frequency and causes the displacement node on the center axis to move towards the small cylindrical section. As the conical section length rises, the increment of resonance frequency reduces and tends to a stable value of 360 Hz while the displacement of the node on the center axis becomes lager and gradually approaches 1.5 mm. Furthermore, the amplitude of the output terminal is stable at 16.18 μm under 220 V peak-to-peak (77.8 V_{RMS}) sinusoidal potential excitation. After that, a prototype was fabricated and validated experiments were conducted. The experimental results are consistent with that of theory and simulations. It provides theoretical basis for the design and optimization of small-size, large-amplitude, and high-power composite transducers.

Keywords: equivalent circuit; composite transducer; quarter-wave; prestressed bolt; finite element analysis.

1. Introduction

A sandwich piezoelectric ceramic transducer converts high-frequency alternating voltage into mechanical vibration through employing inverse piezoelectric effect and its longitudinal eigenmode. These transducers generally consist of a piezoelectric ceramic stack, a front mass which can double as a waveguide, a back mass, and a prestressed bolt (ZHOU *et al.*, 2002). Due to its high mechanical strength, high electromechanical coupling coefficient, high power capacity and stable performance, it is widely used in the fields of underwater acoustics, medical ultrasound, and ultrasonic machining (WEVERS *et al.*, 2005; ASAMI *et al.*, 2015).

Since the amplitude of the vibration generated by a constant cross-section transducer cannot meet the application requirements, a half-wave transducer and horn need to be used simultaneously to amplify amplitude and match impedance. To gain better performance, intensive studies were conducted to raise the amplification coefficient and improve the stress state of the horn. ROSCA *et al.* (2015) presented the design and characterization of an axisymmetric ultrasonic horn held by its circumference, with specified working frequency, amplification factor, and nodal point position. An optimization method based on Webster's horn equation, Hooke's law, and variational calculus theory were employed to design the waveform and corre-

sponding horn shape. Deibel et al. (2013) presented a new methodology to design an ultrasonic amplifier by shape optimization using genetic algorithms and simplex method with specific fitness functions. The results indicated that the proposed optimization method is capable to deliver usable ultrasonic devices meeting the specification of the application. Roopa Rani et al. (2015) performed simulations and experiments to study the thermo-elastic heating of horns made of different materials. They found that the titanium horns are less prone to frequency changes due to thermo-elastic heating effects and they have very long life when subjected to cyclic loads even at high amplitudes. Fu et al. (2012) derived the resonance frequency equation and the amplification coefficient equation of a full-wave barbell horn and performed optimized design for the largest magnification. Based on this, they presented a barbell ultrasonic transducer by adopting equivalent circuit method, which can yield high radiation power and high output amplitude.

The length of the oscillator equipment composed by transducer and high-amplitude horn mentioned earlier is at least one wavelength. These devices have few defects such as unsatisfactory ratio of output power to total mass, higher requirement for the work space, and more energy losses at the junction of the transducer and horn. To remedy these defects and simplify the design and machining processes, Qin et al. (2011) derived the resonance frequency equation of a half-wave sandwich transducer with a quarter-wave conical composite horn based on the equivalent circuit method. Albu-dairi et al. (2013) proposed a longitudinal and torsional ultrasonic vibrator by equivalent circuit method. The front mass of the transducer and the horn were designed as one part to improve the performance and reduce the size of this equipment. The finite element analysis and experiments indicated that satisfied longitudinal and torsional vibration can be gained through the presented ultrasonic unit.

Besides, the prestressed bolt plays an important role in transducer for providing load to prevent interface gapping or excessive tension for piezoelectric ceramics. To simplify the design and given that the additional stiffness and mass of the prestressed bolt are usually much less than that of other parts, the effect of the bolt is generally ignored in the design stage. Sandwiched ultrasonic transducer of longitudinal-torsional compound vibrational modes was studied by Lin (1997). The equivalent circuits without the consideration of the bolt were obtained to describe the longitudinal and torsional vibration and further to design the geometrical parameters of parts. Experimental results indicated that the measured resonance frequency of the transducer was in good agreement with the theoretical value. Arnold (2008) evaluated the effects of the bolt on the resonances of a transducer consisted of a piezoelectric stack and two metal cylindrical parts

theoretically and experimentally. The results demonstrated that the equivalent circuit model taking the bolt into account can provide more accurate prediction of resonance points. DeAngelis et al. (2015) studied the prestressed bolt design for achieving optimal transducer performance, including basic size and strength determination, as well as ensuring adequate thread engagement to the mating horn. Their conclusions provided guidelines for the selection and arrangement of the prestressed bolt in transducer. In addition, the performance of the ultrasonic transducer is influenced by the pre-tightening force of the bolt. Studies indicate that there exists an optical range of the pre-tightening force applied to the prestressed bolt (Arnold et al., 2003; Han et al., 2008). Jiang et al. (2017) found the optimal pre-tightening force for a sandwich transducer by testing the resonance resistance. However, for the half-wave length composite transducer, there are few studies focusing on the influences of the prestressed bolt on the design accuracy in terms of mechanical responses and electrical characteristics.

In this paper, the transducer and the horn were designed as a whole, in other words, an ultrasonic transducer with a quarter-wave taper transition horn was designed based on the equivalent circuit method. Meanwhile, the equivalent circuit of the transducer was adopted to obtain its mechanical responses and electrical characteristics. Then, the finite element analyses were carried out to gain the influences of the prestressed bolt and the conical section length on the dynamic characteristics of this equipment. After that, a prototype was fabricated and measurements were conducted to validate the theory and simulation results. The conclusions can provide guidelines for the design and optimization of small-size, large-amplitude, and high-power sandwich piezoelectric ceramic transducers.

2. Design of the ultrasonic composite transducer

The ultrasonic composite transducer is composed of a front cover, a piezoelectric ceramic stack, a rear cover, and a prestressed bolt. The impacts of prestressed bolt are generally ignored in the initial design of transducers, therefore the front cover, the rear covers, and the piezoelectric ceramic stack can be regarded as solid rods bonded together. The simplified structure of ultrasonic composite transducer, as shown in Fig. 1,
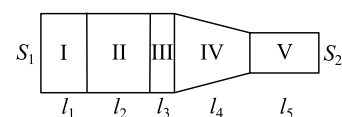

Fig. 1. Structure of the ultrasonic composite transducer. Parameters l_i ($i = 1, 2, ..., 5$) correspond to the lengths of each element, and parameters S_1, S_2 correspond to the areas of two constant cross-section rod.

consists of five segments: the rear cover I, the piezoelectric ceramic stack II, the larger-cylindrical section III, the conical section IV, and the smaller cylindrical section V. The rear cover and the piezoelectric ceramic stack constitute a quarter-wave vibrator employed to generate mechanical vibration. The rest segments constitute a quarter-wavelength composite horn with conical transition, which can be regarded as the front cover of the ultrasonic composite transducer to amplify amplitude and match impedance.

2.1. Equivalent circuit of the ultrasonic composite transducer

The schematic diagram and related parameters for a variable cross-section rod and a piezoelectric ceramic stack are given in Fig. 2. In the figure, S_i ($i = 1, 2, 3$), F_j, v_j ($j = 1, 2, 3, 4$) are the cross-sectional areas, external forces, and external velocities, respectively. For the piezoelectric ceramic stack, V is the excitation voltage.
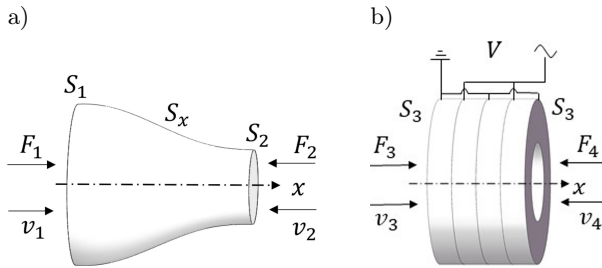

Fig. 2. Schematic diagram for an arbitrary cross-section rod (a) and a piezoelectric ceramic stack (b).

According to Newton's law and the analogy between mechanical vibration and electrical resonance, the equivalent circuits for variable cross-section rod and piezoelectric ceramic stack are provided in Fig. 3. In the latter, the velocity and force on the surfaces of these parts are described as electrical current and voltage, respectively (SHERRIT et al., 1999; DAHIYA et al., 2009; MASON, 1948). In the figure, C_0 is the clamped capacitance of piezoelectric ceramic chip, p is the number of ceramic chips in piezoelectric ceramic stack and n is the electro-mechanical conversion coefficient. The mechanical impedances of these parts are represented
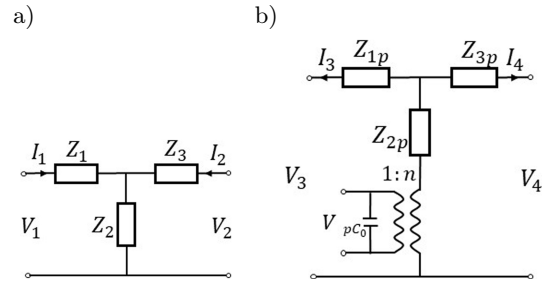

Fig. 3. Equivalent circuit for arbitrary cross-section rod (a) and piezoelectric ceramic stack (b).

by equivalent electrical impedances, which can be calculated as follow:

$$
\begin{cases}
Z_1 = \dfrac{\rho c}{2jk}\left(\dfrac{\partial S}{\partial x}\right)_{(x=0)} + \dfrac{\rho c\lambda S_1}{jk}\cot\lambda l - \dfrac{\rho c\lambda\sqrt{S_1 S_2}}{jk\sin\lambda l}, \\[2ex]
Z_2 = \dfrac{\rho c\lambda\sqrt{S_1 S_2}}{jk\sin\lambda l}, \\[2ex]
Z_3 = \dfrac{\rho c}{2jk}\left(\dfrac{\partial S}{\partial x}\right)_{(x=l)} + \dfrac{\rho c\lambda S_2}{jk}\cot\lambda l - \dfrac{\rho c\lambda\sqrt{S_1 S_2}}{jk\sin\lambda l},
\end{cases}
\tag{1}
$$

$$
\begin{cases}
Z_{1p} = Z_{3p} = j\rho c_e S\tan\left(\dfrac{k_e l}{2}\right), \\[2ex]
Z_{2p} = \dfrac{\rho c_e S}{j\sin(k_e l)},
\end{cases}
\tag{2}
$$

where ρ is the density of the material, $k = \omega/c$ is the wave number, ω is the angular frequency, c is the longitudinal wave velocity, S is the cross-sectional area as a function of x, $\lambda^2 = k^2 - \frac{1}{\sqrt{S}}\frac{\partial^2(\sqrt{S})}{\partial x^2}$, c_e is the equivalent longitudinal wave velocity in the piezoelectric ceramic stack, and $k_e = \omega/c_e$. For the segment with uniform cross-section, $S_1 = S_2 = S$, Eq. (1) can be simplified as $Z_1 = Z_3 = j\rho c S\cdot\tan\left(\frac{kl}{2}\right)$, $Z_2 = \frac{\rho c S}{j\sin(kl)}$.

According to the force and velocity continuous transmission law, the equivalent circuit diagram of the ultrasonic composite transducer can be obtained through connecting the equivalent circuit of each part, as shown in Fig. 4. Since the external loads of the transducer are difficult to determine, it is the usual procedure to regard the transducer as unloaded,
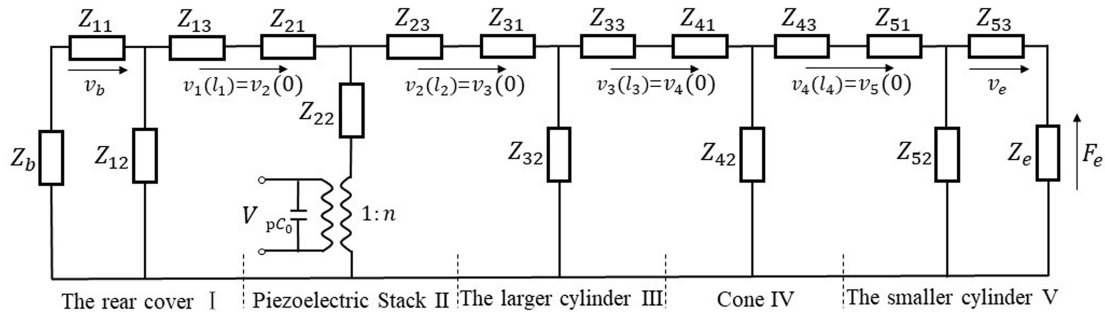

Fig. 4. Equivalent circuit diagram of the ultrasonic composite transducer.

i.e. $Z_b = 0$, $Z_e = 0$, $F_e = 0$. In the figure, the equivalent impedances can be gained according to Eqs (1) and (2), where $N = \sqrt{\frac{S_1}{S_2}}$, $\alpha = \frac{N-1}{Nl}$

$$Z_{i1} = Z_{i3} = j\rho_i c_i S_1 \tan\left(\frac{k_i l_i}{2}\right), \tag{3}$$

$$Z_{i2} = \frac{\rho i c_i S_1}{j \sin k_i l_i} \quad (i = 1, 3), \tag{4}$$

$$Z_{21} = Z_{23} = Z_{1p}, \tag{5}$$

$$Z_{22} = Z_{2p}, \tag{6}$$

$$Z_{41} = \rho_3 c_3 S_1 \left(\frac{1}{j \sin k_3 l_4} - \frac{\alpha}{jk_3}\right) - \frac{\rho_3 c_3 \sqrt{S_1 S_2}}{j \sin k_3 l_4}, \tag{7}$$

$$Z_{42} = \frac{\rho_3 c_3 \sqrt{S_1 S_2}}{j \sin k_3 l_4}, \tag{8}$$

$$Z_{43} = \rho_3 c_3 S_2 \left(\frac{1}{j \tan k_3 l_4} + \frac{\alpha N}{jk_3}\right) - \frac{\rho_3 c_3 \sqrt{S_1 S_2}}{j \sin k_3 l_4}, \tag{9}$$

$$Z_{51} = Z_{53} = j\rho_i c_i S_2 \tan\left(\frac{k_3 l_5}{2}\right), \tag{10}$$

$$Z_{52} = \frac{\rho_3 c_3 S_2}{j \sin k_3 l_5}. \tag{11}$$

There is a cross-section in the transducer where the vibration displacement is equal to zero. This cross-section is defined as nodal plane. The nodal plane of the composite transducer is designed at the interface between the quarter-wave vibrator and the quarter-wave composite horn, i.e. $v_2(l_2) = v_3(0) = 0$. Thus, the following equations can be obtained according to Fig. 4 and the Kirchhoff circuit formula

$$v_b(Z_{11}+Z_{12})-v_2(0)Z_{12}=0, \tag{12}$$

$$-v_b Z_{12}+v_2(0)(Z_{12}+Z_{13}+Z_{21}+Z_{22})=-nV, \tag{13}$$

$$nV - v_2(0)Z_{22} = v_4(0)Z_{22}, \tag{14}$$

$$v_4(0)(Z_{32}+Z_{33}+Z_{41}+Z_{42})-v_5(0)Z_{42}=0, \tag{15}$$

$$-v_4(0)Z_{42}+v_5(0) \\ \cdot (Z_{42}+Z_{43}+Z_{51}+Z_{52}) + v_e Z_{52}=0, \tag{16}$$

$$-v_5(0)Z_{52}+v_e(Z_{52}+Z_{53})=0. \tag{17}$$

According to Eqs (3)–(11) and (15)–(17), for the right side of the nodal plane, the resonance frequency equation and the velocity ratio equation of the quarter-wave composite horn with conical transition can be obtained as follow:

$$\tan k_3 l_5 = \cot k_3 l_4 + \frac{\alpha N}{k_3} \\ - \frac{1}{\sin^2 k_3 l_4 \left(\cot k_3 l_3 + \cot k_3 l_4 - \frac{\alpha}{k_3}\right)}, \tag{18}$$

$$\frac{v_e}{v_4(0)} = \frac{S_1 \left(\cot k_3 l_3 + \cot k_3 l_4 - \frac{\alpha}{k_3}\right)}{\sqrt{S_1 S_2}\cot k_3 l_3}. \tag{19}$$

According to Eqs. (3)–(11) and (13)–(17), the velocity ratio equation of the composite transducer can be calculated as:

$$\frac{v_e}{v_b} = \frac{\rho_2 c_2 S_1 \cos k_1 l_1 \sin k_3 l_3 \sin k_3 l_4}{\rho_3 c_3 \sqrt{S_1 S_2} \sin k_2 l_2 \cos k_3 l_5} \\ \cdot \left(\cot k_3 l_3 + \cot k_3 l_4 - \frac{\alpha}{k_3}\right). \tag{20}$$

For the quarter-wave vibrator, the right terminal of the equivalent circuit can be considered as open circuit resulted from the existence of nodal plane, as shown in Fig. 5. The resonance frequency equation of this part can be obtained by the condition that the total reactance in the loop is zero, i.e. $Z_{m1} + Z_{21} + Z_{22} = 0$, where $Z_{m1} = R_{m1} + jX_{m1}$ is the input impedance on the left side of the piezoelectric ceramic stack. For the constant cross-section rear cover without mechanical load, Z_{m1} can be simplified as $Z_{m1} = jX_{m1} = j\rho_1 c_1 S_1 \tan k_1 l_1$. Therefore, the resonance frequency equation of the quarter-wave vibrator can be gained:

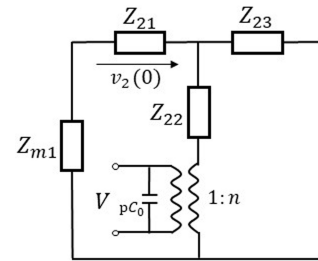$$\tan k_1 l_1 \tan k_2 l_2 = \frac{\rho_2 c_2}{\rho_1 c_1}. \tag{21}$$

Fig. 5. Equivalent circuit for the left part of the nodal plane.

As shown above, the frequency equations of this kind composite transducer are gained through equivalent circuit method. Based on these equations, the geometrical parameters of parts can be calculated according to specific design frequency and partial given data. After that, the equivalent circuit of the transducer also is employed to extract its mechanical responses and electric characteristics.

2.2. Material and size determination of the ultrasonic composite transducer

The resonance frequency of the ultrasonic composite transducer was designed at 20 kHz to meet the ap-

plication requirements and to obtain comprehensive performance. The duralumin and the 45 steel were adopted to manufacture the front cover and the rear cover, respectively. This is benefit for the transmission of energy to the front-end surface. The material of prestressed bolt is stainless steel. The piezoelectric material is PZT-8, for its advantages such as high tensile strength, high mechanical quality factor, high electromechanical coupling coefficient and low dielectric loss, meeting well with the application requirements for strong electric field, large amplitude, and long-time operation.

The piezoelectric ceramic element is a solid limited-dimension piezoelectric cylinder for 3D coupling vibration essentially (ZHANG *et al.*, 2015). For the sake of design accuracy, the coupling propagation velocity of longitudinal wave is calculated through the apparent elastic method (MORI *et al.*, 1977), and is adopted to solve the resonance frequency equation. The longitudinal apparent elastic constant of the isotropic piezoelectric ceramic cylinder can be calculated by (REN, 1983):

$$E_Z = \left\{ S_{33}^E \left[1 + \frac{2\sigma_{13}\sigma_{31}(1+\sigma_{12})}{R_j^2/(a^2\omega^2\rho_2 S_{11}^E) - (1-\sigma_{12}^2)} \right] \right\}^{-1}, \quad (22)$$

where S_{ij}^E ($i = 1, 3$, $j = 1, 3$) is elastic compliance constant, $\sigma_{12} = -S_{12}^E/S_{11}^E$, $\sigma_{13} = -S_{13}^E/S_{11}^E$, ρ_2 is the density of the piezoelectric material, a is the radius, ω is the angular frequency, R_j is the root of radial resonance frequency equation corresponding to fundamental frequency.

The coupling propagation velocity of longitudinal wave in the piezoelectric ceramic stack can be obtained according to the apparent elastic theory while considering the coupling vibration of the piezoelectric ceramic stack and can be expressed as follow:

$$c_Z = \sqrt{\frac{E_Z}{\rho_2}}. \quad (23)$$

The primary parameters of materials and the coupling propagation velocity of longitudinal wave in PZT-8 are given in Table 1. In addition, the piezoelectric matrix $[e]$, the stiffness matrix $[c]$, and the dielectric matrix $[\varepsilon]$ of PZT-8 are defined by Eqs (24)–(26). The piezoelectric ceramic stack consists of four thin electrodes and four PZT-8 elements and the electrode material can be regarded as PZT-8 material as the thickness of an electrode is far less than that of a PZT-8 element. Therefore, the thickness of the rear cover can be calculated as 18 mm via Eq. (21). As for the quarter-wave composite horn with conical transition, the length of the smaller cylindrical section l_5 can be obtained according to the conical section length l_4 via Eq. (18) while the length of the larger cylindrical section is defined as 6 mm. The corresponding values of l_4 and l_5 employed in finite element analysis are shown in Table 2

$$[e] = \begin{bmatrix} 0 & 0 & 0 & 0 & 10.3 & 0 \\ 0 & 0 & 0 & 10.3 & 0 & 0 \\ -4.1 & -4.1 & 14.1 & 0 & 0 & 0 \end{bmatrix} \text{C/m}^2, \quad (24)$$

$$[c] = \begin{bmatrix} 14.9 & 8.11 & 8.11 & 0 & 0 & 0 \\ 8.11 & 14.9 & 8.11 & 0 & 0 & 0 \\ 8.11 & 8.11 & 13.2 & 0 & 0 & 0 \\ 0 & 0 & 0 & 3.13 & 0 & 0 \\ 0 & 0 & 0 & 0 & 3.13 & 0 \\ 0 & 0 & 0 & 0 & 0 & 3.4 \end{bmatrix} \cdot 10^{10} \text{ N/m}^2, \quad (25)$$

$$[\varepsilon] = \begin{bmatrix} 7.97 & 0 & 0 \\ 0 & 7.97 & 0 \\ 0 & 0 & 5.31 \end{bmatrix} \cdot 10^{-9} \text{ F/m}. \quad (26)$$

Table 2. The smaller cylindrical section length and the conical section length.

l_4 [mm]	l_5 [mm]	l_4 [mm]	l_5 [mm]
8	57.2	32	43.7
12	55.1	36	41.1
16	53.0	40	38.3
20	50.7	44	35.4
24	48.5	48	32.2
28	46.2	52	28.8

Table 1. Material parameters.

Material	Density [kg/m³]	Young modulus [GPa]	Poisson's ratio	Velocity [m/s]	Coupling velocity [m/s]
45 steel	7850	210	0.28	5172	–
PZT-8	7600	–	–	3120	3045
Duralumin	2780	71	0.34	5054	–
Stainless steel	7750	193	0.31	4990	–

3. Finite element analysis of the ultrasonic composite transducer

The rear cover, the piezoelectric ceramic stack, and the front cover are connected by a prestressed bolt to constitute a complete transducer. In order to reduce the complexity of theoretical design, prestressed bolt is usually ignored in the design procedure, although it has effects on the dynamic characteristics of the composite transducer. To reveal the influences of the prestressed bolt and conical section length on the vibration characteristics (namely the resonance frequency, the displacement distribution, the output amplitude, and the maximum equivalent stress) of the transducer, ANSYS Workbench was adopted to carry out modal and harmonic response analyses.

Taking the effective electromechanical coupling coefficient and the mechanical strength of the bolt into account, M12 stainless steel bolt was used. Twenty-four models of ultrasonic composite transducers were established depending on the conical section length and the existence of prestressed bolts. The detailed size parameters are given in Table 3.

Table 3. Sandwich transducer oscillator ministries size and materials.

Section		Outer diameter [mm]	Length [mm]	Amount
The rear cover		38	18	1
PZT-8 element		38	5	4
Electrode		38	0.3	4
The front cover	Larger cylinder	38	6	1
	Cone	–	l_4	
	Smaller cylinder	19	l_5	
Prestressed bolt	Nut	18	10	1
	Screw	12	47	

3.1. Analysis of resonance frequency

It is well known that the best performance of a transducer is achieved when it works at the resonance state. In this case, the resonance frequency and the mode shape of a composite transducer can be obtained by modal analysis. In simulation models, the structures of the composite transducers are shown in Fig. 6. The piezoelectric ceramic stack consists of four piezoelectric ceramics and the polarization directions of two adjacent ones are opposite to achieve excitation. SOLID 226 Element with 20 nodes was employed to mesh piezoelectric ceramics and SOLID 187 Element with 10 nodes was adopted to mesh the rear cover and the front cover. Meanwhile, it is assumed that there is
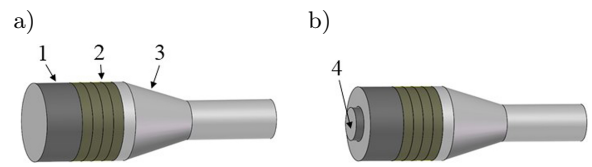

Fig. 6. Simulation models: (a) transducer without the prestressed bolt, (b) transducer with the prestressed bolt; 1 – rear cover, 2 – piezoelectric ceramic stack, 3 – front cover, 4 – prestressed bolt.

no separation in the interfaces between different parts under working condition, thus the contact types of interfaces in analysis models were defined as bonded. To gain the undamped natural frequency and mode shape of the transducer, no damping or fixed constraint was defined in the modal analysis. For the models with prestressed bolt, the bolt had no contact with piezoelectric ceramics. Figure 7 shows the result of modal analysis. The resonance frequency and mode shape of the simulated transducer can be obtained through this figure. It indicates that the resonance frequencies of these two models are 19.824 kHz and 20.181 kHz, respectively. In addition, both two models can generate longitudinal vibration.
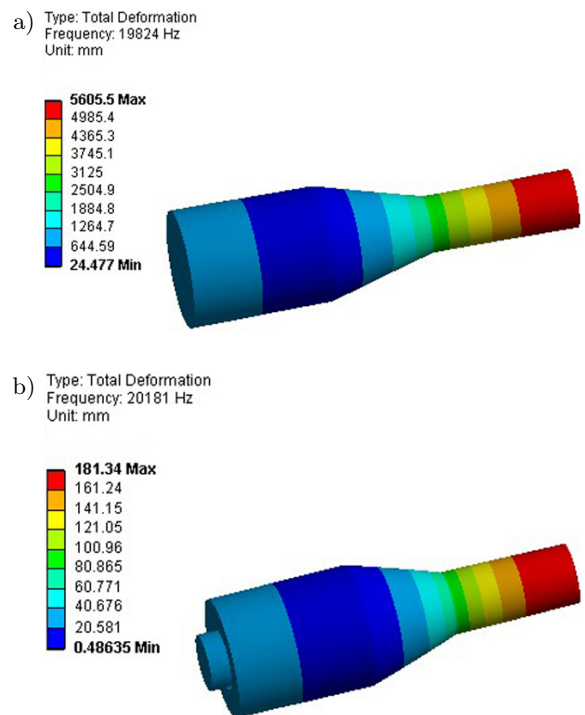

Fig. 7. Longitudinal vibration modes of ultrasonic composite transducers: a) transducer without a prestressed bolt, b) transducer with a prestressed bolt.

The relationship between the resonance frequency and the conical section length is shown in Fig. 8. The resonance frequency of the models without prestressed bolt is slightly lower than the design frequency while that of the models with prestressed bolt is slightly
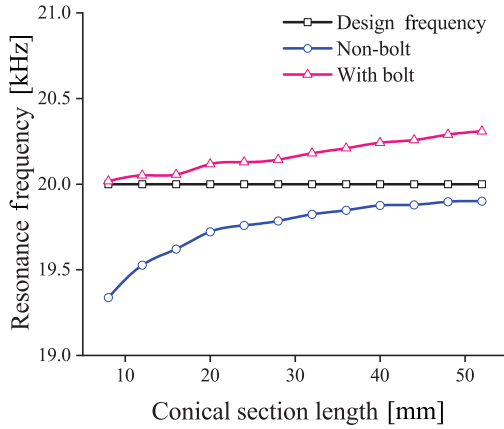
Fig. 8. The resonance frequency *versus* the conical section length.

Fig. 9. Location of the nodal plane *versus* the conical section length.

higher than the design frequency. Hence, the addition of the prestressed bolt can increase the resonance frequency and the increment stabilizes at 360 Hz when the cone length is between 24–40 mm. Furthermore, the resonance frequency for all models increases as the conical section length increases. Errors between simulation result and the design frequency are within 2.36% when the conical section length is greater than 12 mm.

3.2. Analysis of the nodal plane

In most applications, transducer needs to be fixed on the frame or spindle through the flange, and works together with other systems to accomplish the task. The flange needs to be designed at the nodal plane of the transducer to reduce the vibration transferred to the frame or spindle. This can also decrease the energy loss and avoid temperature rising for the transducer. Thus, it is of great significance to locate the nodal plane accurately (KUO, 2008; MATHIESON *et al.*, 2013).

The displacement distributions along center axis and the outline were obtained with the help of the path analysis function of ANSYS Workbench postprocessor. The relationship between the location of the displacement node (namely the distance between the particle whose displacement is zero in the displacement distribution graph and the larger end of the transducer) and the conical section length is shown in Fig. 9. In the figure, for the simulation results, the maximum error in the location of the displacement node on the center axis is 2.3 mm compared with the theoretical value. The occurrence of the error mainly results from the simplification of the vibration modes at the initial design for the transducer. Since the simulation process is more similar to practical condition, the location of the nodal plane can be determined accurately by the simulation results, and it can be optimized by adjusting the thickness of the rear cover. Besides, it can be gained from Fig. 9 that the addition of prestressed bolts will
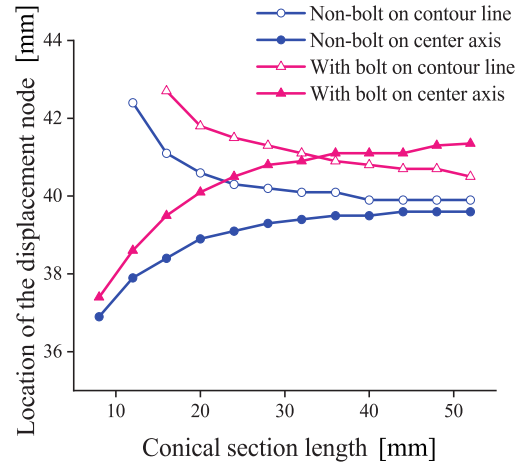
make the displacement nodes on the center axis and on the contour line both move towards to the smaller cylinder section.

It also can be seen from Fig. 9 that the displacement node on the center axis does not coincide with that on the contour line. The value of the former increases as the conical section length increases, while the latter decreases in the same condition. And as the conical section length increases, the values of the displacement nodes tend to be stable. As for models without prestressed bolts, the location of displacement node on the contour line is always greater than that on the center axis. As for models with prestressed bolts, when the conical section length is less than 34 mm, the value of the displacement node on the contour line is greater than that on the axis, while as the conical section length is greater than 34 mm, the conclusion is the other way round. The analyses above also demonstrate that resulted from the transverse vibration of material due to Poisson's effect in the longitudinal vibration process, the amplitudes of particles on the same cross section are not equal and this causes the skewing of nodal plane. Experimental results indicated that it is more reasonable to design the center position of the flange according to the displacement node on the contour line than that on the center axis (ZHAO *et al.*, 2013).

3.3. Analysis of output amplitude and magnifying coefficient

The magnifying coefficient is an important parameter for the transducer and in most applications, the higher the output amplitude is, the better the performance of ultrasonic machining will be. Based on the modal simulation results, the harmonic analyses with a constant damping ratio of 0.007 were carried out to determine the transducer's steady-state response un-

der specific excitation. A fixed constraint was applied to the nodal plane and 220 V peak-to-peak sinusoidal potential was defined according to the polarization directions of piezoelectric ceramics to excite the transducer. The theoretical output amplitude was also obtained through solving the equivalent circuit. The relationship between the output amplitude and the conical section length is shown in Fig. 10. It demonstrates that the conical section length has little influence on output amplitude, while the addition of prestressed bolt will decrease the output amplitude at the smaller end of the transducer. The maximum value of the output amplitude of models with prestressed bolt is 16.44 μm. In addition, the theoretical results are closer to that of the models with prestressed bolt.
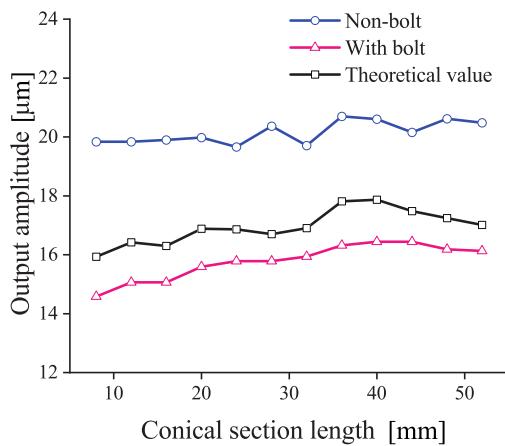

Fig. 10. Amplitude of the output end *versus* the conical section length.

The variable cross-section structure in the smaller side of the ultrasonic composite transducer is adopted to increase output amplitude when the voltage load is certain. Under ideal conditions without energy loss, the amplitude magnifying coefficient of a quarter-wave horn is infinite, so taking the ratio between the velocity of the front end and that of the rear end as reference. The magnifying coefficients obtained by simulation results and gained by theoretical calculation Eq. (20) as the conical section length increases are given in Fig. 11.

It can be drawn from the figure that the magnifying coefficient of the ultrasonic composite transducer decreases with the increase of conical section length. Furthermore, the magnifying coefficient of models with prestressed bolt is larger than that of non-bolt models. As for models without prestressed bolt, simulation results and theory design meet well when the conical section length is among 20–40 mm.

3.4. Analysis of maximum equivalent stress

In order to guarantee adequate mechanical strength of the composite horn, values of the maximum equivalent stress in Von Mises criterion of multi-group mod-
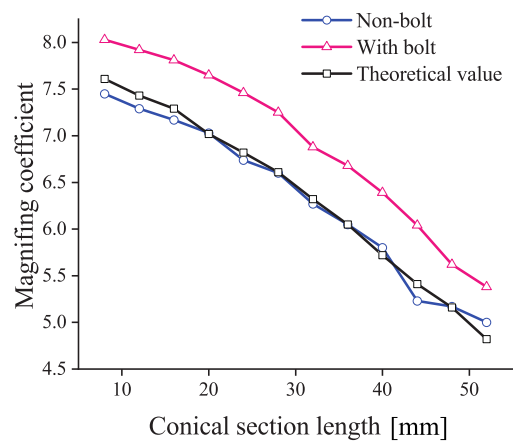

Fig. 11. The magnifing coefficient of amplitude *versus* the conical section length.

els were obtained with the aid of the response analysis module of ANSYS Workbench, as shown in Fig. 12. It can be seen from the figure that the maximum stress of models without prestressed bolt decreases as the conical section length increases, while the maximum stress of models with prestressed bolt changes little. For all models, the maximum equivalent stress occurs at the interface of the conical section and the smaller cylindrical section. It also demonstrates that the maximum equivalent stress of the ultrasonic composite horn is far less than the allowable stress of material, therefore this type of horn can bear large load. Furthermore, larger amplitude can be obtained by increasing the diameter ratio between the two cylindrical sections.
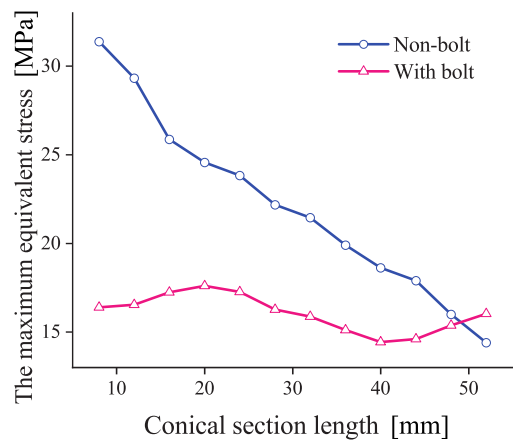

Fig. 12. Maximum equivalent stress *versus* the conical section length.

4. Experimental validation

An ultrasonic composite transducer is fabricated with $l_4 = 32$ mm according to the above simulation results, as shown in Fig. 13. To fix the transducer and measure the displacement at the nodal plane, a flange with 3 mm thickness was machined and its upper sur-
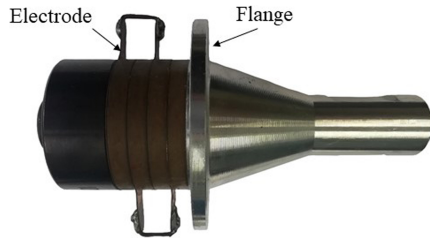
Fig. 13. Fabricated transducer.

face coincides with the nodal plane. Measurements of dynamic characteristics of this prototype were performed to verify the theory and simulation results.

The test setup is shown in Fig. 14. The sinusoidal signal was generated by the function generator (Model AFG3022C, Tektronix, USA) and then was amplified to 220 V through a power amplifier (Model 1040L, E&I, USA). An impedance matching instrument (Model Lo-Hi-Z-8-500, E&I, USA) and a transformer with compensation components were connected between the power amplifier and the transducer to match impedance. Through this, the excitation voltage can be applied to the transducer to drive it. A laser Doppler vibromer (Model LV-S01-ST, Sunny Instruments Singapore Pte Ltd, Singapore) was employed to measure the output amplitude at the small end of the transducer. To gain the magnifying coefficient and verify the nodal plane position of this prototype, the displacements at the back end, the upper and lower surfaces of the flange were also measured. A data acquisition and analysis system software (Model quicksa, Sunny Instruments Singapore Pte Ltd, Singapore) was installed to a PC which communicates with the laser Doppler vibromer. This software was adopted to record and display the measured data. In addition, an impedance analyzer (HIOKI IM3570) was used to gain the impedance curve of the prototype. The uninterruptible power supply provided stable voltage for all instruments in experiments.

Fig. 14. Testing platform: 1 – uninterruptible power supply, 2 – signal generator, 3 – impedance matching, 4 – power amplifier, 5 – the prototype, 6 – transformer with compensation components, 7 – impedance analyzer, 8 – PC, 9 – laser Doppler vibrometer.

The result of the impedance test is shown in Fig. 15. It indicates that the resonance frequency of this prototype is 20176 Hz with an error of 0.88% from the design frequency. The effective electromechanical coupling coefficient is 0.283 which can be calculated through series resonance frequency and parallel resonance frequency. The theoretical impedance curve gained from the equivalent circuit is also provided in Fig. 15. The theoretical result is in agreement with the measured one in term of impedance amplitude, while there exists a small horizontal shifting between them.
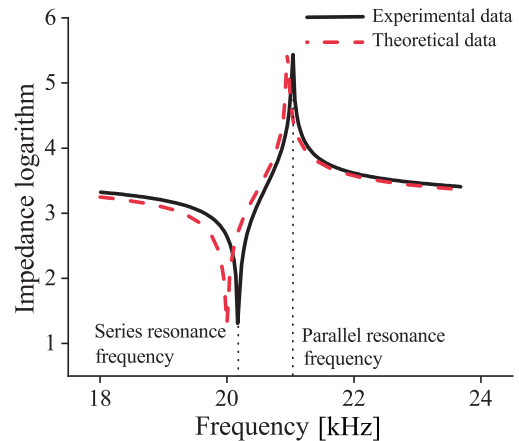

Fig. 15. Theoretical and experimental impedance curves of the prototype.

Figure 16 shows the amplitude measurement result of the output terminal. It demonstrates that this prototype can generate sinusoidal vibration with 15.6 μm amplitude under 220 V peak-to-peak sinusoidal potential excitation. Furthermore, the amplitudes at the output terminal and the back end demonstrate that the magnifying coefficient of this transducer is 6.65. The laser Doppler vibromer did not capture the displacements at the upper and lower surfaces of the flange in experiments due to its limited measurement resolution of 0.1 μm. Thus, it can be considered that the displacements at these two surfaces are both less than
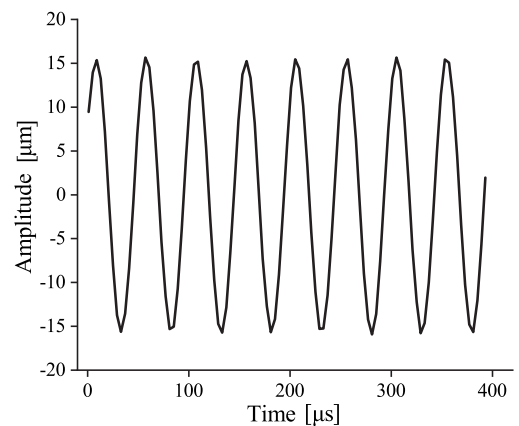

Fig. 16. Measurement result of output amplitude.

Table 4. Theoretical, simulation and experimental results of the prototype.

Feature	Theoretical results	Simulation results of models without bolt	Simulation results of models with bolt	Experimental results
Resonance frequency [Hz]	2000	19824	20181	20176
Output amplitude [μm]	16.9	19.71	15.94	15.6
Magnifying coefficient	6.32	6.27	6.88	6.65
Effective electromechanical coupling coefficient	0.295	–	–	0.283

0.1 μm which can be neglected and the nodal plane position of this prototype is consistent with the theoretical design and simulation results. The comparison among theoretical results, simulation results and experimental results is shown in Table 4.

Table 4 indicates that the experimental results are consistent with the theoretical design and the simulation results of models considering the prestressed bolt within a reasonable error range. As for the discrepancies among them, several possible reasons are as follow: first, the machining error; second, ignoring the prestressed bolt leads to inaccurate definition of stiffness and mass for the transducer; third, the material properties change of the piezoelectric stack under pretightening force is neglected.

5. Conclusions

In this paper, the resonance frequency equations and the expression of displacement amplitude magnification of a half-wave composite transducer were obtained. Multi-group composite transducer models were also established depending on both the existence of prestressed bolt and different values of cone length. Simulations were accomplished to obtain the characteristics such as the resonance frequency, vibration amplitude, the maximum equivalent stress, and the displacement distribution. The influences of the conical section length and the prestressed bolt on the dynamic characteristics were gained. Finally, experiments were carried out to verify the theoretical design and simulation results. The obtained conclusions are as follow:

The equivalent circuit without the consideration of prestressed bolt can be employed to design the composite transducer with satisfied accuracy in terms of resonance frequency, mechanical responses, and electrical characteristics. The simulation results indicate that the addition of the prestressed bolt increases the resonance frequency of the transducer model and causes the displacement node on the center axis to move towards the small cylindrical section. Meanwhile, this decreases the output amplitude and lower the maximum equivalent stress in most cases. The experimental results demonstrate that the simulation models taking the bolt into account can provide more precise prediction of the dynamic characteristics.

For the models considering the prestressed bolt, as the conical section length rises, the resonance frequency of the transducer increases while the magnifying coefficient decreases. When the conical section length is 32 mm, displacement nodes on the center axis and on the contour come to approximately coincide. The conical section length has limited effects on the output amplitude and the maximum equivalent stress. Furthermore, the maximum equivalent stress in the composite horn is less than the allowable stress of the material.

The experimental results demonstrate that the prototype resonates at 20176 Hz with an error of 0.88% to the theoretical resonance frequency and has an effective electromechanical coupling coefficient of 0.283. Under 220 V peak-to-peak sinusoidal potential excitation, the output amplitude of this transducer is 15.6 μm. These results indicate that this prototype can work with satisfied amplitude and high efficiency. The discrepancies among theoretical design, simulation results and experimental results mainly come from the machining error, the inaccurate definition of the stiffness and mass, and the variations of material properties under the bolt preload. The above conclusions can provide theoretical support for the design of small-size, high-power and large-amplitude ultrasonic transducers.

References

1. ALBUDAIRI H., LUCAS M., HARKNESS P. (2013), A design approach for longitudinal-torsional ultrasonic transducers, *Sensors & Actuators A Physical*, **198**(16): 99–106, doi: 10.1016/j.sna.2013.04.024.

2. ARNOLD F.J. (2008), Resonance frequencies of the multilayered piezotransducers, *Journal of the Acoustical Society of America*, **123**(5): 3641–3641, doi: 10.1121/1.2934906.

3. Arnold F.J., Mühlen S.S. (2003), The influence of the thickness of non-piezoelectric pieces on pre-stressed piezotransducers, *Ultrasonics*, **41**(3): 191–196, doi: 10.1016/S0041-624X(03)00096-9.

4. Asami T., Miura H. (2015), Study of ultrasonic machining by longitudinal-torsional vibration for processing brittle materials-observation of machining marks, *Physics Procedia*, **70**: 118–121, doi: 10.1016/j.phpro.2015.08.056.

5. Dahiya R.S., Valle M., Lorenzelli L. (2009), SPICE model of lossy piezoelectric polymers, *IEEE Transactions on Ultrasonics Ferroelectrics and Frequency Control*, **56**: 387–395, doi: 10.1109/ISAF.2008.4693877.

6. Deibel K.R., Wegener K. (2013), Methodology for shape optimization of ultrasonic amplifier using genetic algorithms and simplex method, *Journal of Manufacturing Systems*, **32**(4): 523–528, doi: 10.1016/j.jmsy.2013.05.010.

7. DeAngelis D.A., Schulze G.W., Wong K.S. (2015), Optimizing piezoelectric stack preload bolts in ultrasonic transducers, *Physics Procedia*, **63**: 11–20, doi: 10.1016/j.phpro.2015.03.003.

8. Fu Z.Q., Xian X.J., Lin S.Y., Wang C.H., Hu W.X., Li G.Z. (2012), Investigations of the barbell ultrasonic transducer operated in the full-wave vibrational mode, *Ultrasonics*, **52**(5): 578–586, doi: 10.1016/j.ultras.2011.12.006.

9. Han L., Zhong J., Gao G. (2008), Effect of tightening torque on transducer dynamics and bond strength in wire bonding, *Sensors and Actuators A: Physical*, **141**(2): 695–702, doi: 10.1016/j.sna.2007.10.013.

10. Jiang X.G., Wang K.Q., Zhang D.Y. (2017), Determining the optimal pre-tightening force of a sandwich transducer by measuring resonance resistance, *Applied Acoustics*, **118**: 8–14, doi: 10.1016/j.apacoust.2016.11.009.

11. Kuo K.L. (2008), Design of rotary ultrasonic milling tool using FEM simulation, *Journal of Materials Processing Technology*, **201**(1–3): 48–52, doi: 10.1016/j.jmatprotec.2007.11.289.

12. Lin S.Y. (1997), Sandwiched piezoelectric ultrasonic transducers of longitudinal-torsional compound vibrational modes, *IEEE Transactions on Ultrasonics, Ferroelectrics, and Frequency Control*, **44**(6): 1189–1197, doi: 10.1109/58.656619.

13. Mason W.P. (1948), *Electromechanical Transducers and Wave Filters*, D. Van Nostrand Co.

14. Mori E., Itoh K., Imamura A. (1977), Analysis of a short column vibration by apparent elasticity method and its application, *Ultrasonics International 1977 Conference Proceedings*, 262.

15. Mathieson A., Cardoni A., Cerisola N., Lucas M. (2013), The influence of piezoceramic stack location on nonlinear behavior of Langevin transducers, *IEEE Transactions on Ultrasonics Ferroelectrics and Frequency Control*, **60**(6): 1126–1133, doi: 10.1109/TUFFC.2013.2675.

16. Qin L., Wang L.K., Tang H.Y., Sun B.S. (2011), Resonance frequency equation of a sandwich transducer with complex transformer, *Journal of Vibration and Shock*, **30**(07): 188–191, doi: 10.3969/j.issn.1000-3835.2011.07.035.

17. Ren S.C. (1983), Multi-dimensional couples vibrations of piezoelectric vibrator (I)-Pure piezoelectric vibrator, *Acta Acustica*, **8**(3): 147–158, doi: CNKI:SUN:XIBA.0.1983-03-003.

18. Roopa Rani M., Prakasan K., Rudramoorthy R. (2015), Studies on thermo-elastic heating of horns used in ultrasonic plastic welding, *Ultrasonics*, **55**: 123–132, doi: 10.1016/j.ultras.2014.07.005.

19. Rosca I.C., Pop M.I., Cretu N. (2015), Experimental and numerical study on an ultrasonic horn with shape designed with an optimization algorithm, *Applied Acoustics*, **95**: 60–69, doi: 10.1016/j.apacoust.2015.02.009.

20. Sherrit S. *et al.* (1999), Comparison of the Mason and KLM equivalent circuits for piezoelectric resonators in the thickness mode, *IEEE Ultrasonics Symposium. Proceedings, International Symposium*, **2**: 921–926, doi: 10.1109/ULTSYM.1999.849139.

21. Wevers M., Lafaut J.P., Baert L., Chilibon I. (2005), Low-frequency ultrasonic piezoceramic sandwich transducer, *Sensors & Actuators A Physical*, **122**(2): 284–289, doi: 10.1016/j.sna.2005.05.009.

22. Zhou G.P., Zhang Y.H., Zhang B.F. (2002), The complex-mode vibration of ultrasonic vibration systems, *Ultrasonics*, **40**: 907–911, doi: 10.1016/S0041-624X(02)00224-X.

23. Zhao M.L., Cheng X.L., Zhao B. (2013), Research on the node localization deviation of the ultrasonic amplitude transformer with tool head, *Technical Acoustics*, **32**(3): 253–256, doi: CNKI:SUN:SXJS.0.2013-03-019.

24. Zhang Y.F., Qian F., Cui Y.H., Wang Z. (2015), Resonance-frequency and analysis of three-dimensional coupling vibration for limited-dimension piezoelectric cylinder, *Chinese Journal of Solid Mechanics*, **36**(S): 26–31, doi: CNKI:SUN:GTLX.0.2015-S1-005.